Influence of polyvinylpyrrolidone on optical, electrical, and dielectric properties of poly(2-ethyl-2-oxazoline)-polyvinylpyrrolidone blends

Shubha, A.; Manohara, S.R.; Gerward, L.

Published in:
Journal of Molecular Liquids

Link to article, DOI:
10.1016/j.molliq.2017.09.086

Publication date:
2017

Document Version
Peer reviewed version

Influence of polyvinylpyrrolidone on optical, electrical and dielectric properties of poly(2-ethyl-2-oxazoline)-polyvinylpyrrolidone blends

Shubha A[a], S. R. Manohara[a,*], L. Gerward[b]

[a] Nano-Composites and Materials Research Lab, Department of Physics, Siddaganga Institute of Technology, Tumakuru - 572103, Karnataka, India

[b] Department of Physics, Technical University of Denmark, Lyngby, Denmark (retired)

Abstract

Poly(2-ethyl-2-oxazoline) [PEOX] is blended with polyvinylpyrrolidone [PVP] having a relatively high dielectric constant to improve the optical and electrical properties of the material. PEOX-PVP polymer blends with 0, 20, 40, 60, and 80 wt% PVP are characterized by their structural, optical, electrical and dielectric properties. SEM images and XRD spectra show that PEOX and PVP have a good miscibility and compatibility. XRD also confirms the amorphous structure of the samples. FTIR spectra indicate the presence of hydrogen bonding between PEOX and PVP. The optical energy band gap, E_g^{opt}, and the width of the band tail of localized states in the forbidden band gap, ΔE, as determined by UV-Vis spectroscopy, are changing with PVP content. Electrical and dielectric properties are measured at frequencies from 10 Hz to 8 MHz using an LCR meter. The dielectric constant, the dielectric loss, and the loss tangent (tanδ) decrease, whereas the AC conductivity increases with increasing frequency. PEOX:PVP (80:20 wt%) is an optimum blend with superior properties as compared with pure PEOX. This flexible and high-dielectric-constant polymer blend may have potential application in energy storage.

Keywords: poly(2-ethyl-2-oxazoline), polyvinylpyrrolidone, polymer blend, optical properties, electrical properties, dielectric properties

* Corresponding author: Tel: +91-816-228 2696 (O); Fax: +91-816-228 2994 (O)
E-mail address: sr.manohara@yahoo.com (S. R. Manohara)

1. Introduction

Polymers are of great importance in everyday life because of their advantages over conventional materials (e.g. metals, clay, and wood) with respect to corrosion resistance, lightweight, low-cost production, ease of processing, etc. Polymers have high resistivity and useful dielectric properties. They are used as corrosion protection in electronic devices, and as insulators in circuit boards and electrical cables. They also find applications in sensor technology, molecular electronics, and polymer electrolytes. The electrical properties of polymers are useful in optoelectronic and photonic applications. Studies on water soluble polymers, such as polyvinyl alcohol, polyvinylpyrrolidone, polyethylene oxide, poly(2-ethyl-2-oxazoline), polyacryl amide, etc., has gained significant importance in biomedical applications because of their bio-compatibility [1,2].

Polymer blending is an efficient, and economic method for developing new materials with desired properties [3,4]. The properties of the blends can be tuned by varying composition and processing conditions [5]. Hydrogen bonding and dipole-dipole interactions are the main causes for a good polymer-polymer miscibility and compatibility [6–9]. Polymer blends possess enhanced properties compared to the pristine polymers with respect to corrosion resistance, thermal stability, gas barrier properties, ionic conductivity, and mechanical strength [10–12]. Polymer blends have attracted substantial attention due to their technological importance for a variety of applications such as materials for fuel cells, electrostatic charge dissipation, embedded capacitors, electrochemical sensors, and in photonics, electronics and biotechnology [13–15]. Polymer blends have important applications in pharmacy and biomedicine [16,17]. Non-toxic, bio-degradable and bio-compatible polymer blends have pharmaceutical applications, especially in transdermal drug delivery system (TDDS) [18,19].

Poly(2-ethyl-2-oxazoline) [PEOX] is an efficient optical polymer with good dielectric and mechanical strength, and is considered as potential substitute for polyvinyl alcohol and polyvinylpyrrolidone [PVP] [20]. However, scientific and industrial applications of PEOX are

hampered by its hygroscopic nature, making film processing difficult. On the other hand, blends of PEOX with other polymers may solve these problems and be useful in various optoelectronic devices. PVP has better electrical properties [21] than PEOX. It is non-toxic, inert with good electrical charge storage capacity, transparent, and soluble in broad range of polar solvents. Moreover, it has good environmental stability and adhesion [22]. Being non-toxic, PVP is commonly used in cosmetics, pharmacy and food industry. However, applications in optoelectronics are limited due to brittleness and poor film forming capability. Blending PEOX and PVP should give an improved material with respect to optical and electrical properties.

In the past, polymer blending has been used for improving electrical and mechanical properties of polymer films in various applications [23–36]. The production of petroleum-based polymers and their utilization has increased significantly. But these are not readily biodegradable polymers. The improvement of bio-degradability is an imperative concern in the industrial application of synthetic polymers. Hence, there is an increasing interest for developing biodegradable synthetic polymers. The optical and electrical properties of polymer blends are very important in addition to their mechanical and thermal properties.

An extensive literature survey of the present work has shown that there is almost no information on PEOX-PVP blends. Thus, we have embarked on a systematic study on structural, optical, electrical and dielectric properties of this class of materials. We have reported a simple, environment-friendly and inexpensive method for fabricating biodegradable and water-soluble PEOX-PVP blends. These are characterized by Fourier transform infrared (FTIR) spectroscopy, scanning electron microscopy (SEM), X-ray diffraction (XRD), and ultraviolet-visible (UV-Vis) spectroscopy. The ultraviolet-visible (UV-Vis) spectroscopy was utilised to evaluate various optical properties of blends such as absorption band edge, optical energy band gap, and Urbach energy. The dielectric properties (dielectric constant, dielectric loss, and loss tangent) and AC/DC electrical conductivity of blends have been investigated using LCR meter.

2. Experimental

2.1. Materials

Poly(2-ethyl-2-oxazoline) [PEOX] and polyvinylpyrrolidone [PVP] having average molecular weight of 200,000 and 58,000, respectively, were purchased from Alfa Aesar, USA and used directly. Silver conductive paste was procured from Sigma Aldrich Chemicals, USA. Standard chemicals were used as received.

2.2. Preparation of PEOX-PVP blends

Solid polymer blend films of poly(2-ethyl-2-oxazoline) and polyvinylpyrrolidone were fabricated using a simple solution-blending method. A required quantity of PEOX was dissolved in Milli-Q water at 50 °C using a magnetic stirrer. Similarly, a known quantity of PVP was separately dissolved in Milli-Q water at room temperature. The two solutions were then mixed at 50 °C using a magnetic stirrer to get homogeneous PEOX:PVP blends of compositions 80:20, 60:40, 40:60, and 20:80 wt%. The solutions was then transferred to polypropylene petridishes and kept in vacuum oven for 5 days at 50 °C to evaporate water. The dried films were peeled off from the petridishes, and heated at 70 °C for three hours to remove residual water and facilitate cross-linking. For comparison, pure PEOX and PVP polymer films were also prepared. The thickness of all blend films was about 0.50 mm, as measured by a digital vernier having a resolution of 0.01 mm.

2.3. Scanning electron microscope (SEM) and X-ray diffraction (XRD) studies

The surface morphology of pure and blend films was observed in a TESCAN Vega-3 LMU scanning electron microscope (SEM). X-ray diffraction (XRD) patterns were recorded using a Rigaku SmartLab X-ray diffractometer with Cu K-α radiation (λ = 1.5406 Å, accelerating voltage 40 kV) in the angular range 10–80° (2θ).

2.4. Fourier transform infrared (FTIR) spectroscopy

FTIR transmission spectra were recorded using a Bruker Alpha spectrometer in the wave number range 400–4000 cm^{-1}. Samples were prepared in the following manner: Four drops (about 1 ml) of each blend was placed on a KBr pellet. The solvent was evaporated, keeping the pellet in a vacuum oven at 70 °C for three hour.

2.5. Optical properties

The refractive index of each PEOX-PVP blend was measured in an Abbe refractometer (Model: DR-194, Accuracy: ± 0.5%). Optical spectra were recorded in a double-beam Shimadzu 1800 UV-Vis spectrophotometer (resolution: 1 nm) in the wavelength range 200–800 nm. The absorption coefficient, absorption band edge, optical energy band gap, and the Urbach energy were calculated from the absorbance data.

2.6. Electrical and dielectric properties

Electrical and dielectric properties were measured at room temperature using a fully automated high-precession four-terminal LCR meter (HIOKI-IM3536) and a four-terminal probe (HIOKI-L2000) in the frequency range from 10 Hz to 8 MHz. Silver (Ag) electrodes were deposited on both sides of the blended films for the measurement of their electrical and dielectric properties. This equipment can measure inductance, *L*, capacitance, *C*, and resistance, *R*, plus another fourteen parameters [37]. Contribution of the sample holder for the values of measured parameters can be eliminated, and the basic measurement accuracy of LCR meter is 0.05 %.

3. Theory

3.1. Optical properties

Absorption of light is an important property of polymers. Ultra-violet (UV) radiation may influence unstable bonds, whereas infrared (IR) radiation may be selectively absorbed by functional groups and chemical bonds. The absorption coefficient, α, can be determined from the absorbance, *A*:

$$\alpha = 2.303\left(\frac{A}{t}\right) \qquad (1)$$

where A = log (I_0/I), I_0 and I being the incident and transmitted intensities, 2.303 = ln(10) and t is the thickness of the sample. The absorption coefficient can be represented in a number of ways using the Tauc relation [38–40].

The band gap is the energy difference between the bottom of conduction band and the top of the valance band. The band gap is moderate for semiconductors (< 3 eV) and large for insulators (> 4 eV). It can be classified as direct and indirect, depending on the *k*-vector of the bottom of the conduction band and the top of the valence band. If the *k*-vectors are the same, it is called a "direct gap". If they are different, it is called an "indirect gap". In other words, for a "direct" band gap, the momentum of electrons and holes is the same in the conduction and valence band, and the electron can directly emit a photon. For an "indirect" band gap, a photon cannot be directly emitted, because the electron must pass through an intermediate state, transferring momentum to the crystal lattice.

For large absorbance (α > 10^4 cm^{-1}), the Tauc equation [40] is

$$\alpha h\nu = B(h\nu - E_g^{opt})^n \qquad (2)$$

where α is the linear absorption coefficient, $h\nu$ is the photon energy, B is a constant called the band tailing parameter, E_g^{opt} is the optical energy band gap, and the exponent "n" is the power factor of transition mode, which is dependent upon the nature of the material, whether it is crystalline or amorphous, and type of electronic transition responsible for optical absorption. The specific values of n are 1/2, 3/2, 2, and 3 which corresponds to directly allowed, directly forbidden, indirectly allowed, and indirectly forbidden transitions, respectively [41–43]. For non-crystalline materials, the value of E_g^{opt} can be obtained by plotting $(\alpha h\nu)^{1/n}$ versus $h\nu$ in the high absorption range and extrapolating the linear portion of the graph to zero absorption [43].

For small absorbance (1 $cm^{-1} < \alpha < 10^4\ cm^{-1}$), the absorption coefficient is given by the exponential Urbach law [44]:

$$\alpha = \alpha_0 \exp\left(\frac{h\nu}{\Delta E}\right) \qquad (3)$$

where α_0 is a constant and ΔE denotes the energy of the band tail or sometimes called the Urbach energy, which is often interpreted as width of the band tail of localized states in the forbidden band gap. Taking the natural logarithm on both sides of equation (3),

$$\ln\alpha = \ln\alpha_0 + \frac{h\nu}{\Delta E} \qquad (4)$$

The value of ΔE can be obtained from the slope of linear portion in a graph of $\ln\alpha$ versus $h\nu$.

3.2. Electrical and dielectric properties

The relative permittivity, ε^*, of a material is a complex quantity:

$$\varepsilon^* = \varepsilon' - j\,\varepsilon'' \qquad (5)$$

where ε' is the dielectric constant (i.e. real part of ε^*), and ε'' is the dielectric energy loss (i.e. imaginary part of ε^*). Here, ε' and ε'' represents the energy storage and energy dissipation property, respectively. The loss tangent, $\tan\delta$, or dissipation factor, D, of a material is given by.

$$\tan\delta = \frac{\varepsilon''}{\varepsilon'} \qquad (6)$$

The complex permittivity of a dielectric material can be measured by the parallel-plate-method. A slice of the material with thickness d is placed between two parallel metal plates having surface area A. A parallel RC electric network can model this dielectric structure. The complex electrical impedance, Z^*, is given by equation:

$$Z^* = \frac{R}{1+(\omega C R)^2} - j\frac{\omega C R^2}{1+(\omega C R)^2} = Z' - j\,Z'' \qquad (7)$$

where $\omega = 2\pi f$ is the angular frequency, f is the frequency of the electric field, R and C are resistance and capacitance, and Z' and Z'' are the real and imaginary parts of the complex impedance. The dielectric constant and the dielectric loss are then given by

$$\varepsilon' = \frac{Z''}{\omega C_0 (Z'^2 + Z''^2)} \qquad (8)$$

$$\varepsilon'' = \frac{Z'}{\omega C_0 (Z'^2 + Z''^2)} \qquad (9)$$

where $C_0 = \varepsilon_0 A/d$ is the capacitance of free space between the plates, and ε_0 (= 8.854×10^{-12} F/m) is the permittivity of free space. The loss tangent can also be defined in terms of Z' and Z'':

$$\tan\delta = D = \frac{Z'}{Z''} = \frac{1}{\omega R C} \qquad (10)$$

The dielectric constant, the dielectric loss, and the AC conductivity, σ_{AC}, can be calculated using the equations (11), (12) and (13), respectively.

$$\varepsilon' = \frac{C d}{\varepsilon_0 A} \qquad (11)$$

$$\varepsilon'' = \varepsilon' \tan\delta \qquad (12)$$

$$\sigma_{AC} = \omega \varepsilon_0 \varepsilon'' \qquad (13)$$

All symbols of equations (11) through (13) have the same meaning as in earlier equations. Through built-in programs, the LCR meter directly displays values of the AC conductivity, σ_{AC}, and the absolute permittivity, ε, of material. Software for interfacing with a computer, gives the additional advantage of exporting the data to a predefined MS Excel template. The latter feature greatly facilitates any subsequent graphical or numerical data treatment. Finally, the real (ε') and imaginary (ε'') parts of the relative permittivity are calculated using equation (14) and (12), respectively.

$$\varepsilon' = \frac{\varepsilon}{\varepsilon_o} \qquad (14)$$

where ε_0 is the permittivity of free space. The DC conductivity, σ_{DC}, can be calculated from the measured DC resistance, R_{DC}:

$$\sigma_{DC} = \frac{d}{AR_{DC}} \quad (15)$$

where d is the thickness, and A is the cross-sectional area of the sample.

4. Results and discussion

4.1. Structural characterization

The aim of the XRD study was mainly to confirm the non-crystalline nature of the PEOX-PVP blends. XRD patterns of pure PEOX and PVP, and PEOX-PVP blends are shown in Fig. 1. Pure PEOX and PVP show broad characteristic amorphous peaks at 20°, and 12° and 21° (2θ), respectively. XRD curves of PEOX-PVP blends (80:20, 60:40, 40:60, and 20:80 wt%) show broad peaks at 20°, 11° and 20°, 11.5° and 21°, and 11.6° and 21° (2θ), respectively. However, all blends except PEOX:PVP (80:20 wt%) showed two broad peaks. PEOX:PVP (80:20 wt%) shows one broad peak similar to PEOX, which may be due to the low PVP content. These broad peaks indicate the non-crystalline nature of PEOX, PVP, and their blends. In other words, the absence of sharp peaks in the XRD curves confirmed the amorphous nature of the blends.

FTIR spectra of pure PEOX and PVP, and their blends are presented in Fig. 2. The major absorption peak positions and their assignments are given in the Table 1 [45]. PEOX has a broad absorption peak at 2929 cm^{-1} related to $-CH_2$ asymmetric stretching. The bands at 1631, 1442 and 1035 cm^{-1} are assigned to amide C=O stretching, $-CH_3$ bending, and C–N stretching, respectively. For PVP, the broad absorption peak at 2957 cm^{-1} is attributed to –CH asymmetric stretching. The bands at 1662, 1446, and 1284 cm^{-1} are due to C=O stretching, C–C stretching, and C–N vibration, respectively.

The FTIR spectra of PEOX-PVP blends show almost all of the characteristic peaks of pure PEOX and pure PVP. However, there is a relative shifting of the absorption bands with increasing PVP content, because of hydrogen bonding interactions between $–CH_3$ groups of PEOX and the carbonyl groups of PVP.

SEM pictures [Fig. 3(a-f)] are showing the morphology of pure PEOX, pure PVP and PEOX-PVP blends. The main conclusions are: (1) Pure PEOX and PVP have a smooth surface. (2) There are no structural boundaries in the blends. (3) PVP is well dispersed in the PEOX matrix [Fig. 3(b-e)], indicating that PEOX and PVP are compatible and have a good miscibility because of strong intermolecular interactions. (4) Cluster formation occurs whenever the concentrations of polymers are nearly equal [Fig. 3(c, d)]. (5) Clusters do not appear when either polymer has a low content [Fig. 3 (b, e)], indicating high miscibility for this case.

4.2. Optical properties

The refractive index and the light transmission increase linearly with increasing weight percentage of PVP in the PEOX-PVP blend [Fig. 4]. The increase in refractive index is due to increasing molecular orientation in the blends.

Fig. 5a shows the optical absorption of PEOX and PEOX-PVP blends as functions of wavelength. The $\pi \rightarrow \pi^*$ transition in pure PEOX has an absorption band at 206 nm. The corresponding peak of PEOX-PVP blends is situated in the range 217–237 nm, depending on PVP content. The absorbance in PEOX:PVP (80:20 wt%) is largest, which can be explained by a uniform distribution of PVP in the PEOX matrix. Aggregation of PVP in blends with higher PVP content (i.e. 40, 60, and 80 wt%) resists the absorption of incident light, and will result in less absorption.

The absorption edge, the direct allowed, $E_{\mathrm{d}}^{\mathrm{opt}}$, direct forbidden, $E_{\mathrm{d}}^{\mathrm{opt}}$ (forb.), and indirect allowed, $E_{\mathrm{i}}^{\mathrm{opt}}$, optical energy band gaps, and the Urbach energy, ΔE, can be calculated from plots of α, $(\alpha h\nu)^2$, $(\alpha h\nu)^{2/3}$, $(\alpha h\nu)^{1/2}$, and $\ln\alpha$ versus photon energy, $h\nu$, respectively [Fig. 5(b–

f)]. The absorption edge, and the direct and indirect band gaps were determined by extrapolating the straight-line portions of the curves to zero absorption. ΔE values were obtained from the reciprocal of slopes of the linear portions in the graphs of $\ln\alpha$ versus $h\nu$. It is seen that, the absorbance and the absorption edge are slightly shifted toward smaller wavelength with increasing PVP content.

Values of the optical parameters are given in Table 2. It is seen that the absorption edge, and the direct and indirect band gaps of PEOX-PVP blends are slightly increasing with increasing PVP concentration. The optical parameters are minimum for PEOX:PVP (80:20 wt%). This may be due to the creation of localized energy states in the band gap as a result of compositional disorder and/or the change in the number of available final states [42,46]. This can also be explained due to the increase in the number of unsaturated defects increased the density of final states in the band structure which leads to a decrease of optical band gap [47].

4.3. Electrical and dielectric properties

The frequency dependence of the dielectric constant, ε', and the dielectric loss, ε'', for pure PEOX and PEOX-PVP blends is illustrated in Fig. 6(a, b). The relative experimental error is less than 1%. Below 1 kHz, ε' and ε'' rapidly increases with decreasing frequency for PEOX:PVP (80:20 wt%) and PEOX:PVP (40:60 wt%), whereas there is only a slight increase for the other blends. The large values of ε' and ε'' at low frequencies are caused by either the Maxwell-Wagner effect (an AC current in phase with the applied potential), or DC conductivity due to increasing mobility of charge carriers, or both [48,49]. Above 1 kHz, ε' and ε'' are almost constant for all blends. In the whole frequency range, ε' and ε'' are largest for PEOX:PVP (80:20 wt%) blend.

In general, the trend of ε' decreasing with increasing frequency is observed for most dielectric materials and can be explained by dielectric relaxation. The dielectric constant, ε', is mainly due to electronic or atomic, ionic, orientation, and interfacial or space charge

polarizations, and it increases with increasing polarizability. The dipoles (i.e. polar dielectric molecules) in a material align themselves along an applied electric field. If the electric field is alternating, then the dipoles will keep on changing their direction of alignment. The dipoles need some time to attain equilibrium condition which is called relaxation time. The relaxation time depends on the type of polarization. Orientation polarization has longer relaxation time than atomic or electronic polarization. The materials exhibit high dielectric values at lower frequencies due to the increasing number of dipoles. At high frequencies, only electronic polarization is able to follow the applied field and hence, ε' becomes small.

The dielectric loss, ε'', decreases with increasing frequency because of friction between the dipoles. This frictional effect leads to energy loss, called dielectric loss, which is dissipated as heat in the material. At low frequencies, the dipoles have enough time to orient themselves completely along the direction of the field. Thus, the internal friction and the corresponding dielectric loss are large. The orientation and interfacial polarizations are more effective at the lower frequencies and are responsible for the higher dielectric losses. At high frequencies, the dipoles have less time to orient themselves completely along the direction of the field and undergo less internal friction resulting lower dielectric losses. The electronic and ionic polarizations are more effective at higher frequencies which are responsible for the lower dielectric losses.

The inset graphs (at right-hand side) in Fig. 6(a, b) shows an anomalous behavior of ε' and ε'' as a function of PVP content. The ε' and ε'' for PEOX:PVP (80:20 wt%) are larger than for pure PEOX and other blends. For PEOX:PVP (80:20 wt%), ε' = 3270 and ε'' = 482 at 1 kHz, which is considerably higher than for pure PEOX (ε' = 1136 and ε'' = 42, respectively). The large value of ε' is due to the increasing orientation of dipoles in the direction of field. The effective interaction between $-CH_3$ groups of PEOX and carbonyl groups of PVP reduces the cohesive forces between the macromolecular PEOX and PVP polymer chains, which improve

the segmental mobility in the blend. Hence, more dipoles are developed, increasing ε' of blend with 20 wt% PVP. Due to the larger agglomeration in the blend having higher concentration of PVP, the distance between segments will reduce. Therefore, ε' and ε'' values decreases at higher PVP concentration.

The loss tangent, tanδ, as a function of frequency (Fig. 7) is similar that of ε'', since tanδ is a measure of the dielectric loss in the material. The values of tanδ are higher at lower frequency, decreases with increasing frequency and almost constant a higher frequency. The large values of loss tangent at low frequencies are due to the sum of ionic and interfacial polarization in the blends [50]. The lower values of tanδ at higher frequencies are due to the hindrance for the orientations of dipoles. From the insert graph (at right) of Fig. 7, it can be observed that, tanδ is larger for blends than for pure PEOX, the highest value is observed for PEOX:PVP (80:20 wt%) blend. The intermolecular interaction between PEOX and PVP increases with increasing weight percentage of PVP. The higher values of tanδ are due to the increase in the number of self-associated bonds formed by the intermolecular interaction. However, tanδ is decreasing for higher weight percentage of PVP (> 20 wt%). This may be ascribed to high PVP content in the blend leads to the formation of discrete aggregates which lowers the tanδ.

Fig. 8 shows the frequency dependence of the AC conductivity, σ_{AC}, of pure PEOX and PEOX-PVP blends at room temperature. The σ_{AC} of all samples has strong frequency dependence due to their insulating nature. From the figure it is clear that σ_{AC} of each sample increases linearly with increase of frequency of the applied electric field. Similar behaviors have been reported for other polymer blends [33,51]. This behavior is attributed to the combined effect of interface charge polarization (Maxwell-Wagner-Sillar effect) and intrinsic dipole polarization [36]. According to Maxwell-Wagner-Sillar interfacial model, the interfaces between PEOX and PVP segments acts as potential barrier, and the charge carriers in the segment behaves like charges in a potential well. These charge carriers can effortlessly move within the

polymer segments, but cannot migrate easily between the segments due to resistive interfaces. At low frequencies, there is some possibility for few charge carries to tunnel from one segment to another leading to small amount of electrical conduction. As frequency increases, the tunneling of large number of charge carriers takes place which results in an increase of σ_{AC}. At high frequencies, the charge carriers get sufficient energy to overcome the potential barrier resulting in the larger σ_{AC}.

It is seen in the inset graph (at bottom) of Fig. 8 that, σ_{AC} is maximum for PEOX-PVP blend having 20 wt% PVP. However, the σ_{AC} does not increase with further addition of PVP above 20 wt%. This composition is called the *percolation limit/threshold* of a blend [52,53]. The conductivity of the polymer blend depends on the concentration of filler polymer, the tendency of the filler polymer to aggregate, and the morphology of the matrix polymer. The matrix changes from insulating to partially conducting behavior at 20 wt% PVP due to the formation of a conductive network at percolation. PVP combines with PEOX to form strong aggregates at higher wt% of PVP. These aggregates lead to lower conductivity due to loose clustering, and forming of internal crannies, voids, and nooks, which is confirmed by SEM analysis (Fig. 3). These lead to the poor conductivity of the blend at higher wt% of PVP. Further, the conductivity of PEOX:PVP (40:60 wt%) blend is lower than that of pure PEOX. This may be due to poor interfacial interaction between PEOX and PVP, reducing electronic and dipole polarization.

Fig. 9 shows the DC conductivity, σ_{DC}, of the PEOX-PVP blends as a function of the PVP loading. The figure illustrates an anomalous behavior of σ_{DC} as a function of PVP content. It can be noted that σ_{DC} of pure PEOX (2.78×10^{-10} S/m) increases to about three times (to 7.23×10^{-10} S/m) by adding 20 wt% PVP. The high σ_{DC} in the blend with 20 wt% PVP is due to the formation of a conducting path which made it easier for the electrical charge to hop through. The lower values of σ_{DC} for other blends is due to the reduction of number of conducting paths

when the PVP is added at larger concentration to the PEOX matrix, and also, due to fewer free electrons available for conduction process.

5. Conclusions

It has been found that PVP has a profound effect on structural, optical, electrical and dielectric properties of PEOX-PVP blends. The shift of absorption peaks in the UV-Vis and FTIR spectra confirm the interaction between PEOX and PVP molecules. The SEM images show how addition PVP affects the morphology. The absorption band edge, the direct/indirect optical energy band gap, and the Urbach energy have been measured as a function of the PVP content. The dielectric constant, the dielectric loss and the loss tangent of the blends decrease with increasing frequency of an applied electric field, whereas the AC conductivity increases with increasing frequency.

In inclusion, an optimum amount of 20 wt% PVP significantly improves the performance of pristine PEOX. Thus, PEOX:PVP (80:20 wt%) has superior optical, electrical and dielectric properties. This flexible and high-dielectric-constant material should be helpful in the production of nanocomposites with potential application in energy storage.

Acknowledgments

One of the authors, S. R. Manohara wish to thank the Vision Group on Science and Technology (VGST), Department of Information Technology, Biotechnology and Science & Technology, Government of Karnataka, for providing financial support under project no. KSTePS/VGST/03/CISEE/2015-2016/GRD-470. Manohara is also grateful to Director, Dr. M. N. Channabasappa, and Principal, Dr. Shivakumariah, Siddaganga Institute of Technology (SIT), Tumakuru for providing essential infrastructural facilities for this project. Authors acknowledge the help on FTIR and XRD, and UV-Vis measurements, respectively, of Drs. V. Udayakumar, G Nagaraju, and B. S. Gowrishankar of the Departments of Chemistry and Biotechnology at this institute. The author, Shubha A is thankful to SIT for providing research assistantship under R and D programme of Technical Education Quality Improvement Programme (TEQIP) Phase-II.

References

[1] B. Imre, B. Pukánszky, Compatibilization in bio-based and biodegradable polymer blends, Eur. Polym. J. 49 (2013) 1215–1233.

[2] M.J. Caulfield, G.G. Qiao, D.H. Solomon, Some aspects of the properties and degradation of polyacrylamides, Chem. Rev. 102 (2002) 3067–3084.

[3] I.C. Sauchez, Bulk and interface-thermodynamics of polymer alloys, Rev. Mater. Sci. 13 (1983) 387–412.

[4] I.S. Elashmawi, E.M. Abdelrazek, A.M. Hezma, A. Rajeh, Modification and development of electrical and magnetic properties of PVA/PEO incorporated with MnCl2, Phys. B Condens. Matter. 434 (2014) 57–63.

[5] L.A. Utracki, Polymer blends handbook, Volume 2, Kluwer Academic Publishers, USA, 2003.

[6] S.H. Yuk, S.H. Cho, H.B. Lee, pH-sensitive drug delivery system using OW emulsion, J. Control. Release. 37 (1995) 69–74.

[7] R. Araya Hermosilla, A.A. Broekhuis, F. Picchioni, Reversible polymer networks containing covalent and hydrogen bonding interactions, Eur. Polym. J. 50 (2014) 127–134.

[8] K. Dean, L. Yu, S. Bateman, D.Y. Wu, Gelatinized starch/biodegradable polyester blends: processing, morphology, and properties, J. Appl. Polym. Sci. 103 (2007) 802–811.

[9] Siddaramaiah, T.M. Mruthyunjaya Swamy, Studies on miscibility of sodium alginate/polyethylene glycol blends, J. Macromol. Sci. Part A. 44 (2007) 321–327.

[10] X. Lu, H. Zhang, Y. Zhang, Study on ester-amide exchange reactions between nylon 1010 and ethylene-vinyl acetate rubber with different metal derivatives, J. Polym. Res. 21 (2014) 539.

[11] P. Xu, F. Yang, Modification of phenolic resin composites by hyperbranched polyborate

and polybenzoxazine, Polym. Compos. 33 (2012) 1960–1968.

[12] M.T. Ramesan, T.K. Manoj Kumar, R. Alex, B. Kuriakose, Investigations on the addition of styrene butadiene rubber in natural rubber and dichlorocarbene modified styrene butadiene rubber blends, J. Mater. Sci. 37 (2002) 109–116.

[13] S.H. Liao, C.H. Hung, C.C.M. Ma, C. Yen, Y.F. Lin, C.C. Weng, Preparation and properties of carbon nanotube-reinforced vinyl ester/nanocomposite bipolar plates for polymer electrolyte membrane fuel cells, J. Power Sources. 176 (2008) 175–182.

[14] J. Kwon, H. Kim, Comparison of the properties of waterborne polyurethane/multiwalled carbon nanotube and acid-treated multiwalled carbon nanotube composites prepared byin situ polymerization, J. Polym. Sci. Part A Polym. Chem. 43 (2005) 3973–3985.

[15] H. Pang, T. Chen, G. Zhang, B. Zeng, Z.M. Li, An electrically conducting polymer/graphene composite with a very low percolation threshold, Mater. Lett. 64 (2010) 2226–2229.

[16] F. Croisier, C. Jérôme, Chitosan-based biomaterials for tissue engineering, Eur. Polym. J. 49 (2013) 780–792.

[17] T. Çaykara, S. Demirci, Ö. Kantoğlu, Thermal, spectroscopic, and mechanical properties of blend films of poly(N-vinyl-2-pyrrolidone) and sodium alginate, Polym. Plast. Technol. Eng. 46 (2007) 737–741.

[18] M.M. Feldstein, V.N. Tohmakhchi, L.B. Malkhazov, A.E. Vasiliev, N.A. Platé, Hydrophilic polymeric matrices for enhanced transdermal drug delivery, Int. J. Pharm. 131 (1996) 229–242.

[19] M.M. Feldstein, I.M. Raigorodskii, A.L. Iordanskii, J. Hadgraft, Modeling of percutaneous drug transport in vitro using skin-imitating carbosil membrane, J. Control. Release. 52 (1998) 25–40.

[20] S.R. Manohara, T.N. Rajashekara, A. Shubha, S.S. Subhranshu, M.V. Murugendrappa, P.N. Navya, Preparation, characterization and spectroscopic investigations of PEOX-

PVOH blend films, Sensors & Transducers. 210 (2017) 32–37.

[21] V.V.R.N. Rao, A. Kalpalatha, Electrical conduction mechanism in poly(vinyl pyrrolidone) films, Polymer (Guildf). 28 (1987) 648–650.

[22] R.J. Fried, Polymer Science and Technology, Prentice Hall, N. J., 2000.

[23] A. Rawat, H.K. Mahavar, S. Chauhan, A. Tanwar, P.J. Singh, Optical band gap of polyvinylpyrrolidone/polyacrilamide blend thin films, Indian J. Pure Appl. Phys. 50 (2012) 100–104.

[24] J.L. Acosta, E. Morales, Structural, morphological and electrical characterization of polymer electrolytes based on PEO/PPO blends, Solid State Ionics. 85 (1996) 85–90.

[25] J.Y. Kim, S.H. Kim, Ionic conduction behavior of network polymer electrolytes based on phosphate and polyether copolymers, Solid State Ionics. 124 (1999) 91–99.

[26] K. Rama Mohan, V.B.S. Achari, V.V.R.N. Rao, A.K. Sharma, Electrical and optical properties of (PEMA/PVC) polymer blend electrolyte doped with NaClO4, Polym. Test. 30 (2011) 881–886.

[27] J.R. de Lima, C. Schreiner, I.A. Hümmelgen, C.C.M. Fornari Jr., C.A. Ferreira, F.C. Nart, Charge injection from polyaniline-poly (methylmethacrylate) blends into poly (p-phenylene vinylene), J. Appl. Phys. 84 (1998) 1445–1448.

[28] Y. Wang, X. Jing, Transparent conductive thin films based on polyaniline nanofibers, Mater. Sci. Eng. B Solid-State Mater. Adv. Technol. 138 (2007) 95–100.

[29] M.M. Abdi, H.N.M. Ekramul Mahmud, L.C. Abdullah, A. Kassim, M. Zaki Ab. Rahman, J.L.Y. Chyi, Optical band gap and conductivity measurements of polypyrrole-chitosan composite thin films, Chinese J. Polym. Sci. 30 (2012) 93–100.

[30] S.B. Aziz, O.G. Abdullah, A.M. Hussein, R.T. Abdulwahid, M.A. Rasheed, H.M. Ahmed, S.W. Abdalqadir, A.R. Mohammed, Optical properties of pure and doped PVA:PEO based solid polymer blend electrolytes: two methods for band gap study, J. Mater. Sci. Mater. Electron. 28 (2017) 7473–7479.

[31] G. Patel, M.B. Sureshkumar, Preparation of PAM/PVA blending films by solution-cast technique and its characterization: A spectroscopic study, Iran. Polym. J. 23 (2014) 153–162.

[32] S.A. Ghani, S.H.M. Din, J.A. Jalil, Properties of poly(vinyl chloride)/poly(ethylene oxide)/polyaniline conductive films: The effect of poly(ethylene glycol) diglycidyl ether, Polym. Plast. Technol. Eng. 55 (2016) 929–936.

[33] M.T. Ramesan, V.K. Athira, P. Jayakrishnan, C. Gopinathan, Preparation, characterization, electrical and antibacterial properties of sericin/poly(vinyl alcohol)/poly(vinyl pyrrolidone) composites, J. Appl. Polym. Sci. 133 (2016) 43535.

[34] L.I. Buruiana, E. Avram, V.E. Musteata, A. Filimon, Optical and electronic properties of quaternized polysulfone/polyvinyl alcohol blends in relation to structure of the polymers, Mater. Chem. Phys. 177 (2016) 442–454.

[35] M.T. Ramesan, K. Surya, Studies on electrical, thermal and corrosion behaviour of cashew tree gum grafted poly(acrylamide), Polym. from Renew. Resour. 7 (2016) 81–100.

[36] M.T. Ramesan, Processing characteristics and mechanical and electrical properties of chlorinated styrene-butadiene rubber/fly ash composites, J. Thermoplast. Compos. Mater. 28 (2015) 1286–1300.

[37] HIOKI, Instruction Manual of IM3536 LCR Meter, HIOKI E.E. Corporation, Japan, 2015.

[38] J. Tauc, Amorphous and Liquid Semiconductors, Springer US, 1974.

[39] J. Tauc, R. Grigorovici, A. Vancu, Optical properties and electronic structure of amorphous germanium, Phys. Status Solidi. 15 (1966) 627–637.

[40] J. Tauc, A. Menth, States in the gap, J. Non. Cryst. Solids. 8 (1972) 569–585.

[41] H.S.S. Abd El-Kader, F. H. Osman, W. H. Ragab, M.A.F. A. M. Rizk, M. S. Basha, Electrical and optical properties of polyvinyl alcohol thin films doped with metal salts, J.

Polym. Mater. 21 (2004) 49–60.

[42] N.F. Mott, E.A. Davis, Electronic processes in non-crystalline materials, 2nd ed., Clarendon Press, Oxford; Oxford University Press, New York, 1979.

[43] N. Chopra, A. Mansingh, G.K. Chadha, Electrical, optical and structural properties of amorphous V2O5-TeO2 blown films, J. Non. Cryst. Solids. 126 (1990) 194–201.

[44] F. Urbach, The long-wavelength edge of photographic sensitivity and of the electronic absorption of solids, Phys. Rev. 92 (1953) 1324.

[45] D.L. Pavia, G.M. Lampman, G.S. Kriz, J.A. Vyvyan, Introduction to Spectroscopy, 5th ed., Cengage Learning, USA, 2015.

[46] M.M. El-Samanoudy, A.H. Ammar, Some physical and optical properties of the a-Se85SbxS15–x film system, Phys. Status Solidi. 187 (2001) 611–621.

[47] C.H. Cholakis, W. Zingg, M. V. Sefton, Effect of heparin-pva hydrogel on platelets in a chronic canine arterio-venous shunt, J. Biomed. Mater. Res. 23 (1989) 417–441.

[48] H.F. Abd-El-Messieh, S. L. Naguib, Electrical conductivity and dielectric behavior of some poly(alkyl methacrylate)s/polyvinylpyrrolidone blends, Polym. Plast. Technol. Eng. 44 (2005) 1591–1606.

[49] A.L.G. Saad, A.M. Hassan, M.A. Youssif, M.G.M. Ahmed, Studies of electrical properties of some fire-retarding poly(vinyl chloride) compositions, J. Appl. Polym. Sci. 65 (1997) 27–35.

[50] P. Jayakrishnan, M.T. Ramesan, Synthesis, characterization and electrical properties of Fe3O4/poly(vinyl alcohol-co-acrylic acid) nanocomposites, AIP Conf. Proc. 1620 (2014) 165–172.

[51] A.M. Bishai, F.A. Gamil, F.A. Awni, B.H.F. Al-Khayat, Dielectric and mechanical properties of poly(vinyl chloride)–dioctylphthalate systems, J. Appl. Polym. Sci. 30 (1985) 2009–2020.

[52] J. Petzelt, D. Nuzhnyy, V. Bovtun, M. Savinov, M. Kempa, I. Rychetsky, Broadband

dielectric and conductivity spectroscopy of inhomogeneous and composite conductors, Phys. Status Solidi. 210 (2013) 2259–2271.

[53] Z.M. Dang, J.K. Yuan, J.W. Zha, T. Zhou, S.T. Li, G.H. Hu, Fundamentals, processes and applications of high-permittivity polymer-matrix composites, Prog. Mater. Sci. 57 (2012) 660–723.

Figure captions:

Fig. 1. X-ray scattering curves of pure PEOX and PVP, and PEOX-PVP blends (2θ = scattering angle). [Color figure can be viewed in the online issue].

Fig. 2. FTIR spectra of pure PEOX and PVP, and PEOX-PVP blends. [Color figure can be viewed in the online issue].

Fig. 3. SEM images (scale mark 5 μm) showing surface morphology of pure PEOX and PVP, and PEOX-PVP blends. (a) Pure PEOX, (b) 80:20 wt%, (c) 60:40 wt%, (d) 40:60 wt%, (e) 20:80 wt%, and (f) pure PVP.

Fig. 4. Refractive index of PEOX-PVP blends as a function of the PVP content in wt%.

Fig. 5. (*a*) Absorbance versus wavelength, (*b*) absorption coefficient versus photon energy, (*c*) $(\alpha h\nu)^2$ versus photon energy, (*d*) $(\alpha h\nu)^{2/3}$ versus photon energy, (*e*) $(\alpha h\nu)^{1/2}$ versus photon energy, and (*f*) $\ln\alpha$ versus photon energy for pure PEOX and PEOX-PVP blends. [Color figures can be viewed in the online issue].

Fig. 6. Frequency dependence of the relative permittivity for pure PEOX and PEOX-PVP blends. (A) Pure PEOX, (B) 80:20 wt%, (C) 60:40 wt%, (D) 40:60 wt%, and (E) 20:80 wt%. [Color figures can be viewed in the online issue]. The inset graphs on the right-hand side are showing ε' and ε'', respectively, at 1 kHz as functions of the PVP content in wt%.

(a) Real part, ε'.

(b) Imaginary part, ε''.

Fig. 7. Frequency dependence of loss tangent, tanδ, for PEOX-PVP blends. (A) Pure PEOX, (B) 80:20 wt%, (C) 60:40 wt%, (D) 40:60 wt%, and (E) 20:80 wt%. The inset graph on the right-hand side is showing tanδ at 1 kHz as a function of the PVP content in wt%.

Fig. 8. Frequency dependence of the AC conductivity, σ_{AC}, for PEOX-PVP blends. (A) Pure PEOX, (B) 80:20 wt%, (C) 60:40 wt%, (D) 40:60 wt%, and (E) 20:80 wt%. The inset graph at the bottom is showing σ_{AC} at 1 kHz as a function of the PVP content in wt%.

Fig. 9. DC conductivity, σ_{DC}, of PEOX-PVP blends as a function of the PVP content in wt%.

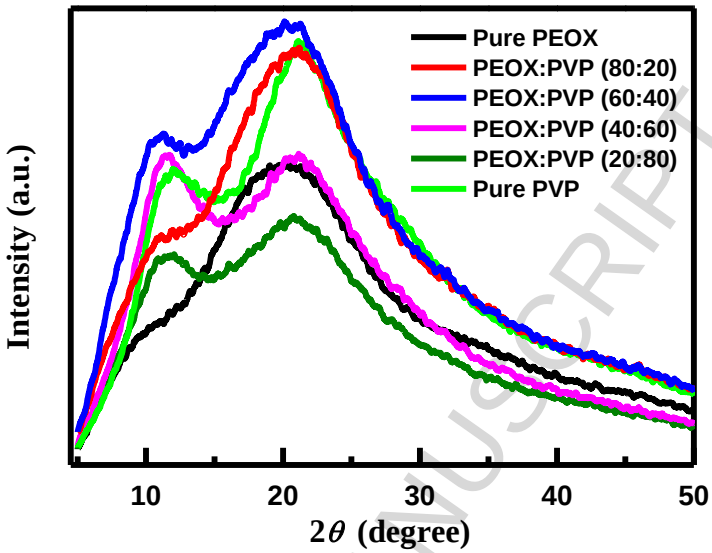

Fig. 1. X-ray scattering curves of pure PEOX and PVP, and PEOX-PVP blends (2θ = scattering angle). [Color figure can be viewed in the online issue].

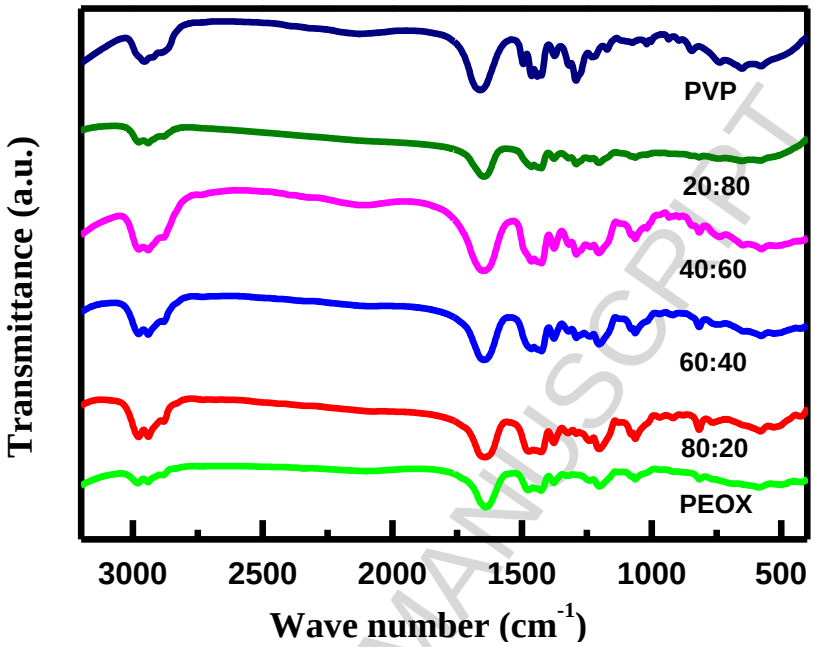

Fig. 2. FTIR spectra of pure PEOX and PVP, and PEOX-PVP blends. [Color figure can be viewed in the online issue]

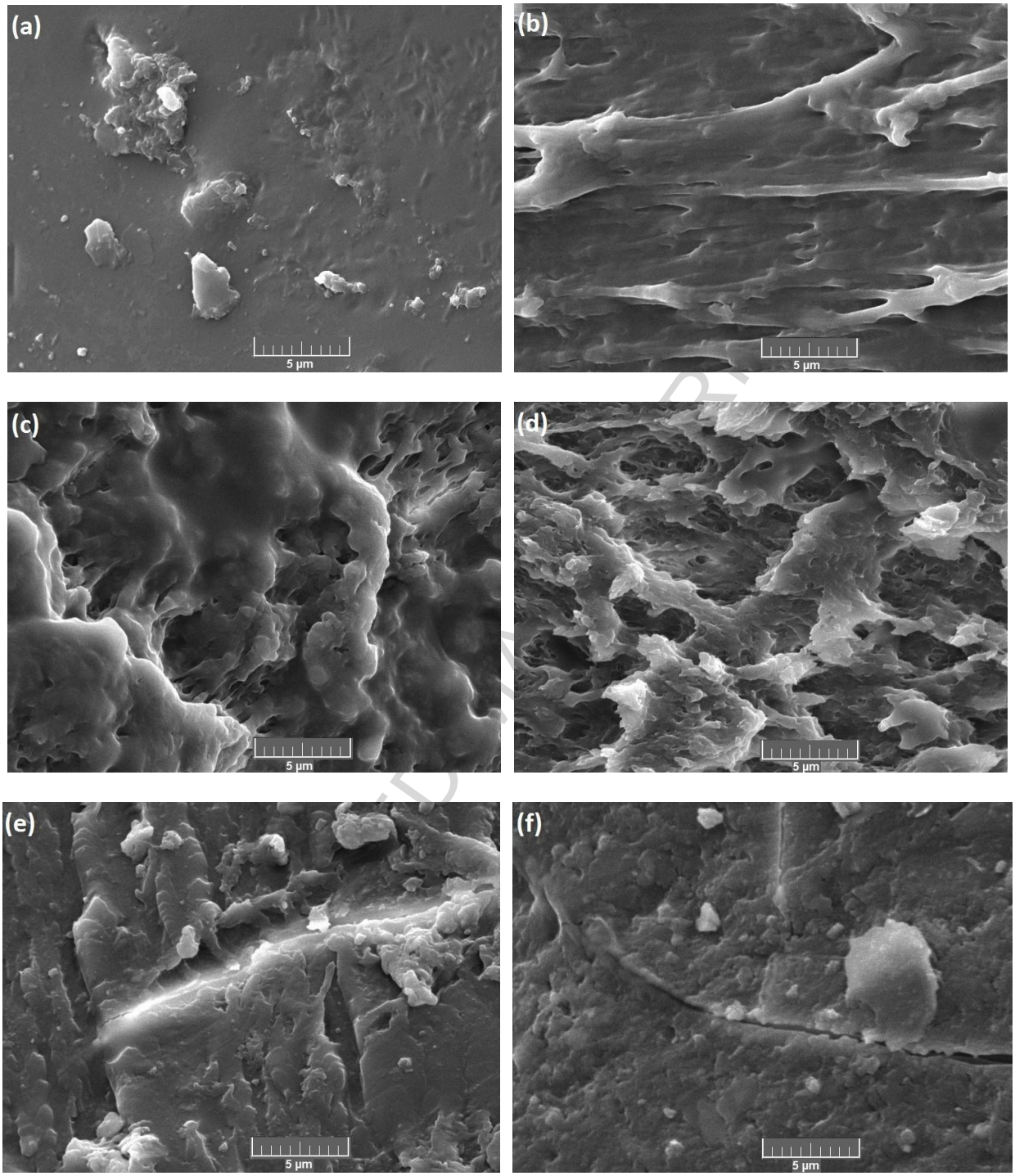

Fig. 3. SEM images (scale mark 5 µm) showing surface morphology of pure PEOX and PVP, and PEOX-PVP blends. (a) Pure PEOX, (b) 80:20 wt%, (c) 60:40 wt%, (d) 40:60 wt%, (e) 20:80 wt%, and (f) pure PVP.

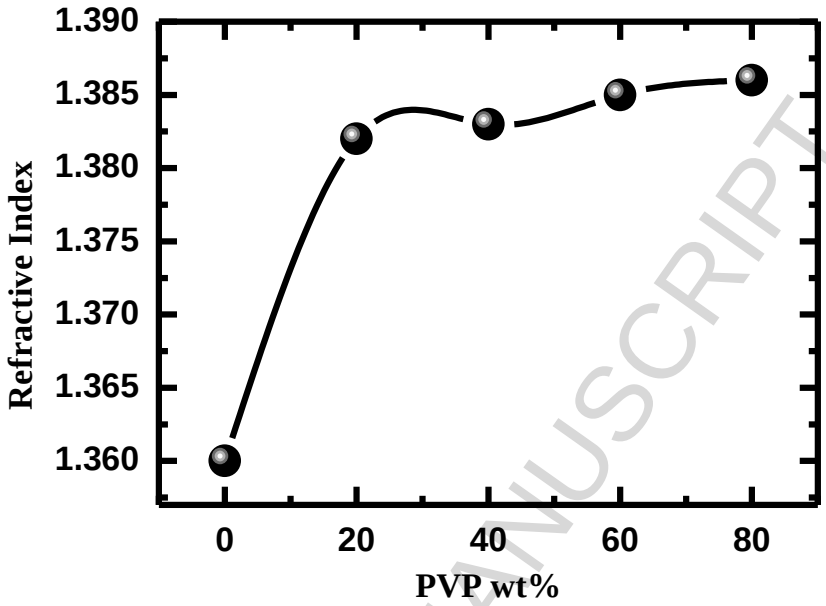

Fig. 4. Refractive index of PEOX-PVP blends as a function of the PVP content in wt%.

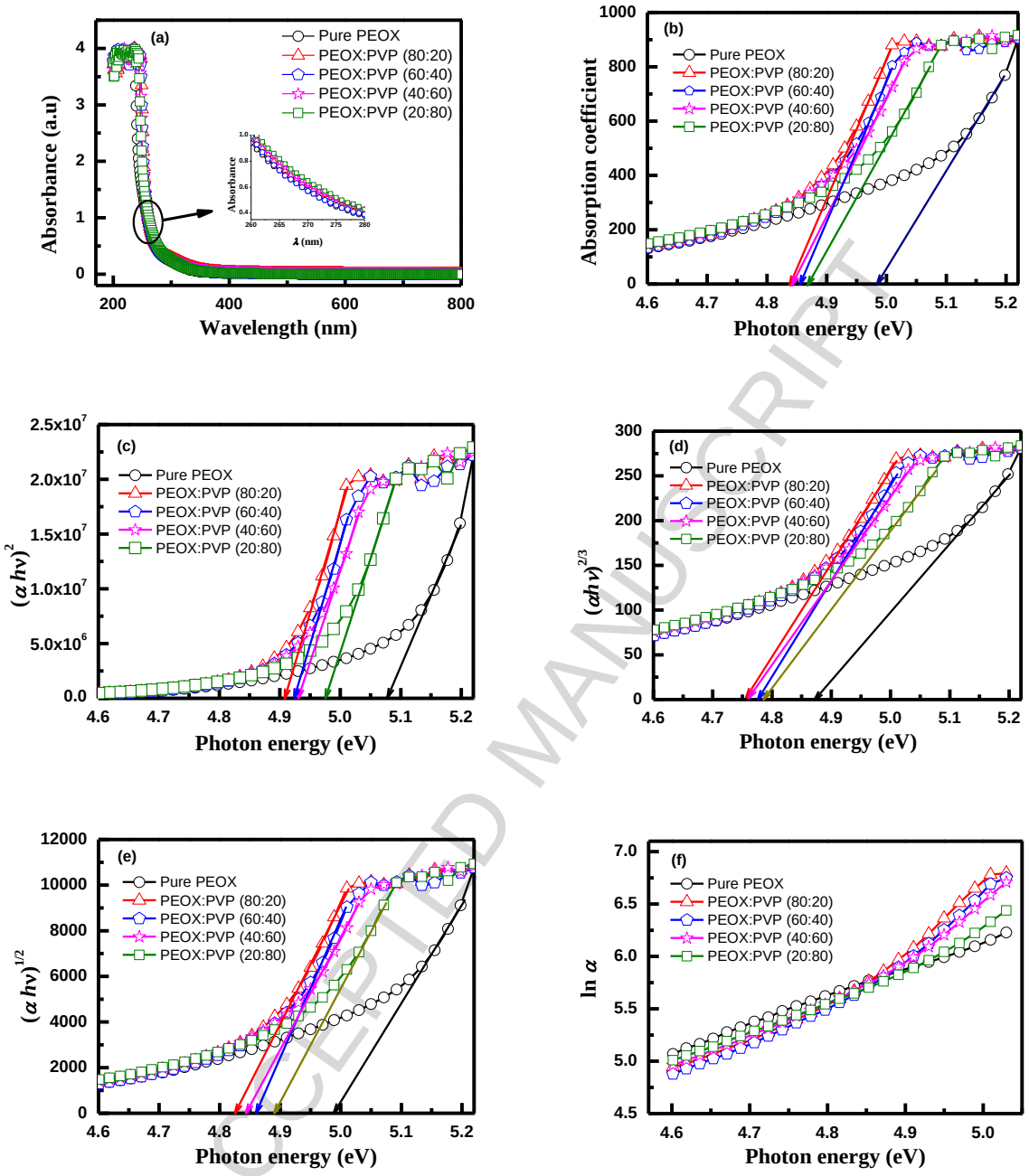

Fig. 5. (*a*) Absorbance versus wavelength, (*b*) absorption coefficient versus photon energy, (*c*) $(\alpha h\nu)^2$ versus photon energy, (*d*) $(\alpha h\nu)^{2/3}$ versus photon energy, (*e*) $(\alpha h\nu)^{1/2}$ versus photon energy, and (*f*) $\ln\alpha$ versus photon energy for pure PEOX and PEOX-PVP blends. [Color figures can be viewed in the online issue].

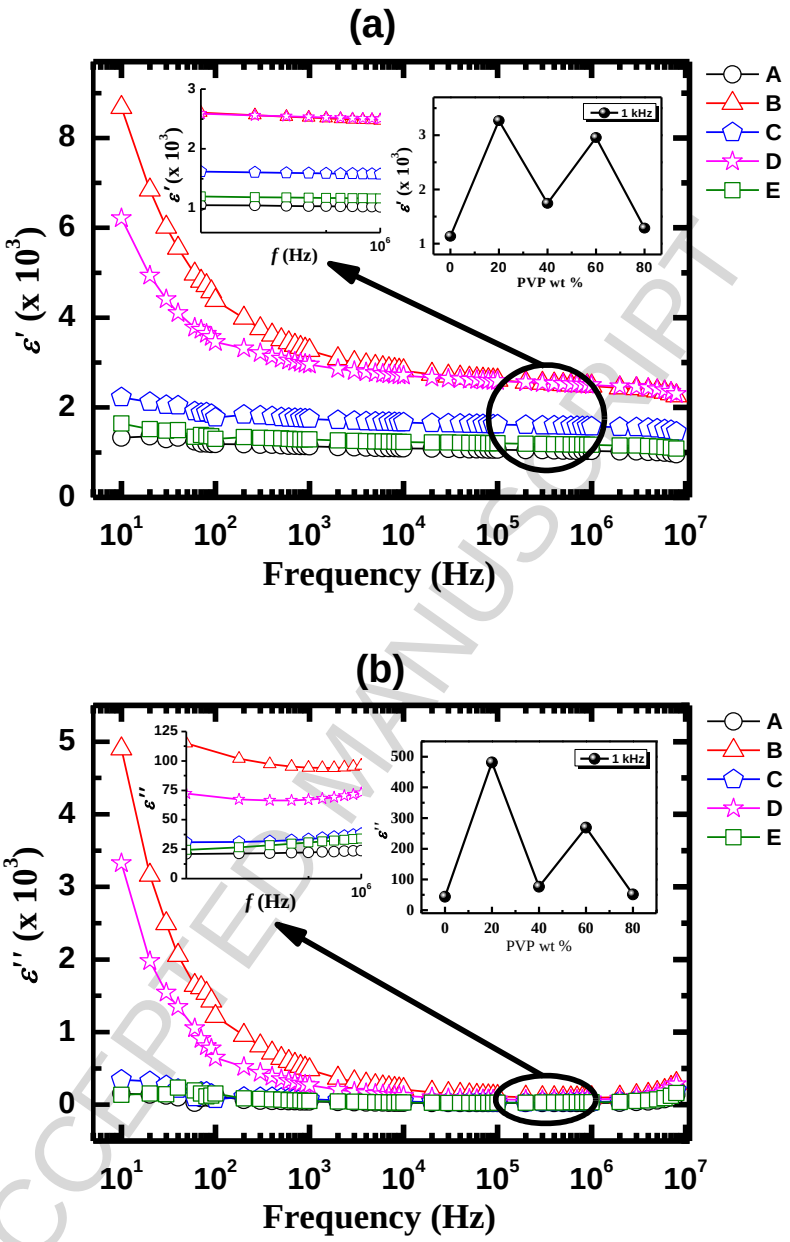

Fig. 6. Frequency dependence of the relative permittivity for pure PEOX and PEOX-PVP blends. (A) Pure PEOX, (B) 80:20 wt%, (C) 60:40 wt%, (D) 40:60 wt%, and (E) 20:80 wt%. [Color figures can be viewed in the online issue]. The inset graphs on the right-hand side are showing ε' and ε'', respectively, at 1 kHz as functions of the PVP content in wt%.

(a) Real part, ε'.

(b) Imaginary part, ε''.

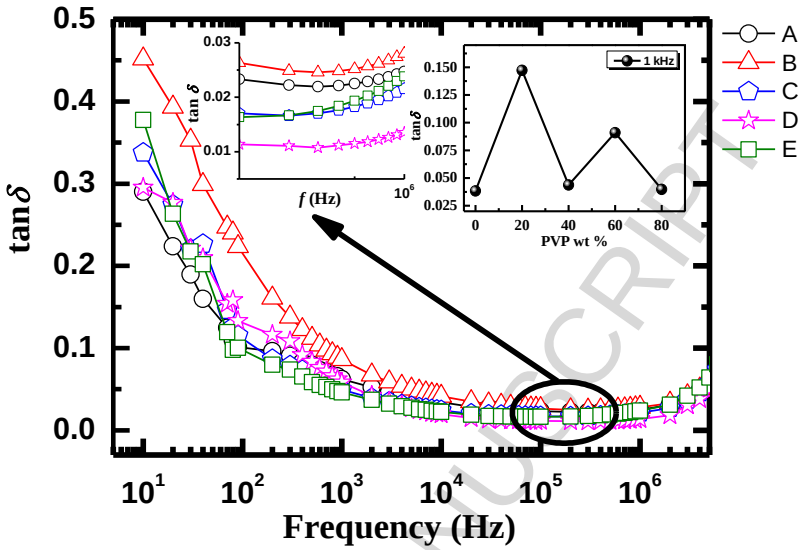

Fig. 7. Frequency dependence of loss tangent, tanδ, for pure PEOX and PEOX-PVP blends. (A) Pure PEOX, (B) 80:20 wt%, (C) 60:40 wt%, (D) 40:60 wt%, and (E) 20:80 wt%. The inset graph on the right-hand side is showing tanδ at 1 kHz as a function of the PVP content in wt%.

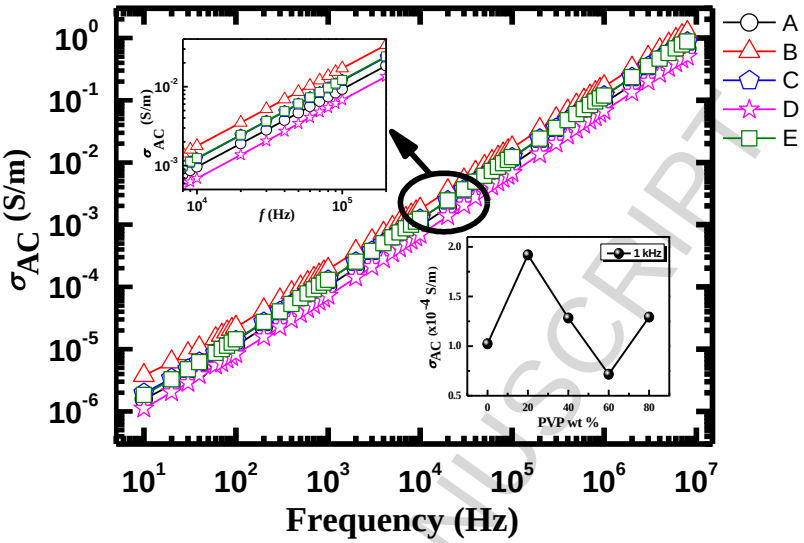

Fig. 8. Frequency dependence of the AC conductivity, σ_{AC}, for pure PEOX and PEOX-PVP blends. (A) Pure PEOX, (B) 80:20 wt%, (C) 60:40 wt%, (D) 40:60 wt%, and (E) 20:80 wt%. The inset graph at the bottom is showing σ_{AC} at 1 kHz as a function of the PVP content in wt%.

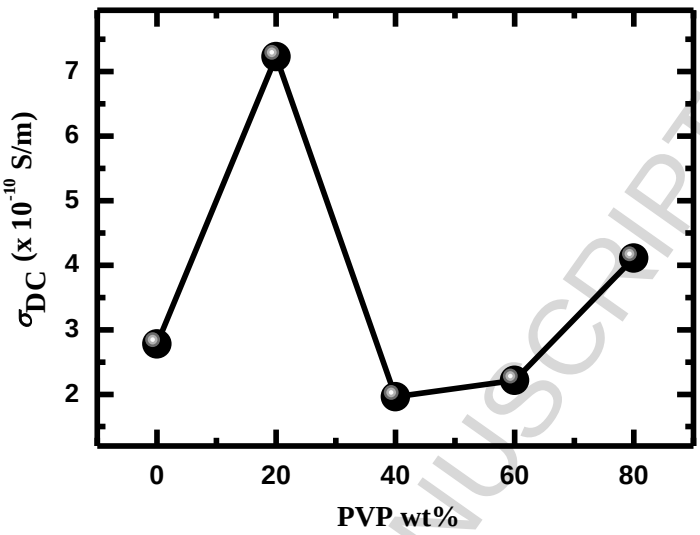

Fig. 9. DC conductivity, σ_{DC}, of PEOX-PVP blends as a function of the PVP content in wt%.

Table 1. Wave numbers and peak assignments of FTIR spectra of pure PEOX and PVP, and PEOX-PVP blends.

Wave no. (cm^{-1})	Peak assignment (PEOX)	Wave no. (cm^{-1})	Peak assignment (PVP)	80:20 (wt%)	60:40 (wt%)	40:60 (wt%)	20:80 (wt%)
2929	$–CH_2$ asymmetric stretching	2957	–CH asymmetric stretching	2940	2940	2941	2939
1631	Amide C=O stretching	1662	C=O stretching	1643	1645	1647	1644
1442	$–CH_3$ bending	1446	C–C stretching	1427	1428	1425	1424
1035	C–N stretching	1284	C–N vibration	1203	1201	1203	1202

Table 2. Absorption edge, direct optical energy band gap (allowed and forbidden), indirect optical energy band gap (allowed), and Urbach energy of pure PEOX and PEOX-PVP blends.

Sample	Absorption edge (eV)	E_d^{opt} [a] (eV)	E_d^{opt} (forb.)[b] (eV)	E_i^{opt} [c] (eV)	ΔE [d] (eV)
Pure PEOX	4.98	5.08	4.87	4.99	0.38
PEOX:PVP (80:20 wt%)	4.84	4.91	4.75	4.82	0.22
PEOX:PVP (60:40 wt%)	4.86	4.92	4.78	4.86	0.23
PEOX:PVP (40:60 wt%)	4.84	4.93	4.76	4.84	0.26
PEOX:PVP (20:80 wt%)	4.87	4.98	4.79	4.89	0.31

[a] Direct allowed optical energy band gap.

[b] Direct forbidden optical energy band gap.

[c] Indirect allowed optical energy band gap.

[d] Urbach energy or width of the band tail of localized states in the forbidden band gap.

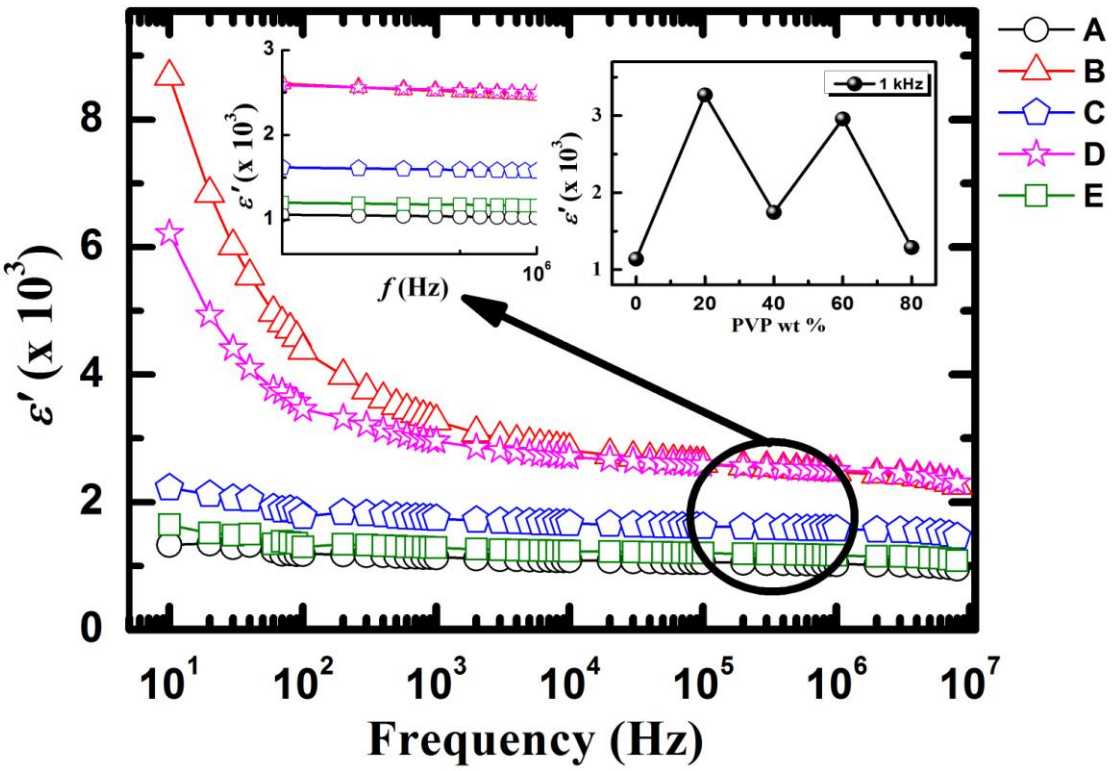

Graphical Abstract

Highlights

- PEOX-PVP blends were prepared by a simple, economic and environment-friendly method.
- Absorption band edge, band gap, and Urbach energy vary with PVP content.
- ε', ε'' and loss tangent of PEOX-PVP blends decreases with increasing frequency.
- AC conductivity of the PEOX-PVP blends increases with increasing frequency.
- PEOX:PVP (80:20 wt%) shows superior optical, electrical, and dielectric properties.